The T#2-$Li_{2/3}Co_{2/3}Mn_{1/3}O_2$ System. 2. Its Electrochemical Behavior

F. Tournadre,[†] L. Croguennec,*[,†] I. Saadoune,[†,‡] M. Morcrette,[§] P. Willmann,[||] and C. Delmas[†]

Institut de Chimie de la Matière Condensée de Bordeaux−CNRS and Ecole Nationale Supérieure de Chimie et Physique de Bordeaux, Université Bordeaux I, 87 Av. du Dr A. Schweitzer, 33608 Pessac Cedex, France, L.C.M.E., Département de Chimie, Faculté des Sciences et Techniques, Av. Abdelkrim, B.P. 549, 40000 Marrakech, Morocco, L.R.C.S., Laboratoire de Réactivité et Chimie des Solides, Université Picardie Jules Verne, 33 Rue Saint Leu, 80000 Amiens, France, and Centre National d'Etudes Spatiales, 18 Av. Edouard Belin, 31401 Toulouse Cedex 4, France

Received November 17, 2003

Electrochemical lithium deintercalation from the metastable T#2-$Li_{2/3}Co_{2/3}Mn_{1/3}O_2$ system has been investigated. The single-phase domains that separate the voltage plateaus observed on the cycling curve have been characterized by in situ and ex situ X-ray diffraction. T#2, T#2′, and $O6_1$ phases are formed during the first charge and then $O6_1$, T#2′, T#2, and $O6_2$ during the first discharge, and the $O6_2$ structure is finally maintained for the whole composition range during the next cycles. The T#2 stacking, also reported for the T2-$Li_{2/3}Ni_{1/3}Mn_{2/3}O_2$ phase by Dahn et al. and for the T#2-Li_xCoO_2 phase ($0.52 < x \leq 0.72$) by Carlier et al., is characterized by oxygen ions that do not occupy the positions of a same triangular lattice and by very distorted tetrahedral sites for lithium ions. The O6 stacking is observed for small and large lithium compositions, corresponding to $O6_1$ and $O6_2$ phases, respectively. Because the formation of the $O6_2$ phase is irreversible, it is assumed to be different from the $O6_1$ and from the O6-Li_xCoO_2 ($0.33 < x \leq 0.42$) previously reported.

Introduction

Lamellar $LiMO_2$ phases can exhibit two different stackings, depending on the synthesis method: O3-type structure for high-temperature thermal treatment and "O2"-type structure for low-temperature ionic exchange reaction. All the phases which will be considered in this paper are named according to the packing designation commonly used for the layered oxides: the letters P, T, and O describe the alkali ion environment (prismatic, tetrahedral, or octahedral, respectively) and the numbers 1, 2, 3, etc. give the number of slabs required to describe the hexagonal cell.[1] A few years ago, Paulsen et al. studied O2-$LiMnO_2$ obtained by ion exchange from the P2 sodium-containing phase and showed that, contrary to O3-$LiMnO_2$, the O2-$LiMnO_2$ phase does not convert into a spinel structure upon cycling.[2] But, because of poor electrochemical performances, this phase was shown not to be promising as positive electrode material for Li-ion batteries. Then, these authors focused their interest on O2-$LiCoO_2$[3] and T#2-$Li_{2/3}Ni_{1/3}Mn_{2/3}O_2$[4−6] systems. In the same time in our laboratory some of us studied also the O2-$LiCoO_2$ system.[7−10] O2-$LiCoO_2$ and T#2-$Li_{2/3}Ni_{1/3}Mn_{2/3}O_2$ are obtained by ion exchange of Na^+ by Li^+ in P2-$Na_{2/3}CoO_2$ and P2-$Na_{2/3}Ni_{1/3}Mn_{2/3}O_2$, respectively. The main difference between these two systems is that the exchange of Na^+ by Li^+ in P2-$Na_{2/3}CoO_2$ is associated with the reduction of Co^{4+} to Co^{3+}, whereas no redox process occurs during the exchange in P2-$Na_{2/3}Ni_{1/3}Mn_{2/3}O_2$. This is due to the difference in stability between the oxidation states of metal ions: indeed Co^{3+}, Ni^{2+}, and Mn^{4+} ions are stable whereas Co^{4+} ions are not, leading thus to the formation of O2-$LiCo^{3+}O_2$ and T#2-$Li_{2/3}Ni^{2+}{}_{1/3}Mn^{4+}{}_{2/3}O_2$ from P2-$Na_{2/3}Co^{3+,4+}O_2$ and P2-$Na_{2/3}Ni^{2+}{}_{1/3}Mn^{4+}{}_{2/3}O_2$. The electrochemical performances of O2-$LiCoO_2$ and T#2-$Li_{2/3}Ni_{1/3}Mn_{2/3}O_2$ in lithium batteries are also highly different: while O2-$LiCoO_2$ can be cycled within the $0 \leq x < 1$ lithium composition range, T#2-$Li_{2/3}Ni_{1/3}Mn_{2/3}O_2$ can only be cycled within the 1/3

* Corresponding author. Tel.: +33-5-4000-2234. Fax: +33-5-4000-6698. E-mail: crog@icmcb.u-bordeaux.fr.
[†] Université Bordeaux I.
[‡] L.C.M.E.
[§] Université Picardie Jules Verne.
[||] Centre National d'Etudes Spatiales.

(1) Delmas, C.; Fouassier, C.; Hagenmuller, P. *Physica* **1980**, *99B*, 81.
(2) Paulsen, J. M.; Thomas, C. L.; Dahn, J. R. *J. Electrochem. Soc.* **1999**, *146*, 3560.
(3) Paulsen, J. M.; Mueller-Neuhaus, J. R.; Dahn, J. R. *J. Electrochem. Soc.* **2000**, *147*, 508−516.
(4) Paulsen, J. M.; Thomas, C. L.; Dahn, J. R. *J. Electrochem. Soc.* **2000**, *147*, 861−868.
(5) Paulsen, J. M.; Dahn, J. R. *J. Electrochem. Soc.* **2000**, *147*, 2478−2485.
(6) Paulsen, J. M.; Thomas, C. L.; Dahn, J. R. *J. Electrochem. Soc.* **2000**, *147*, 2862−2867.
(7) Carlier, D.; Saadoune, I.; Suard, E.; Croguennec, L.; Ménétrier, M.; Delmas, C. *Solid State Ionics* **2001**, *144*, 263−276.
(8) Carlier, D.; Saadoune, I.; Ménétrier, M.; Delmas, C. *Electrochem. Soc.* **2002**, *149*, A1136.
(9) Carlier, D.; Croguennec, L.; Ceder, G.; Ménétrier, M.; Shao-Horn, Y.; Delmas, C. *Inorg. Chem.* **2004**, *43* (3), 914−922.
(10) Carlier, D.; Van der Ven, A.; Delmas, C.; Ceder, G. *Chem. Mater.* **2003**, *15*, 2651−2660.

10.1021/cm035177h CCC: $27.50
Published on Web 03/16/2004

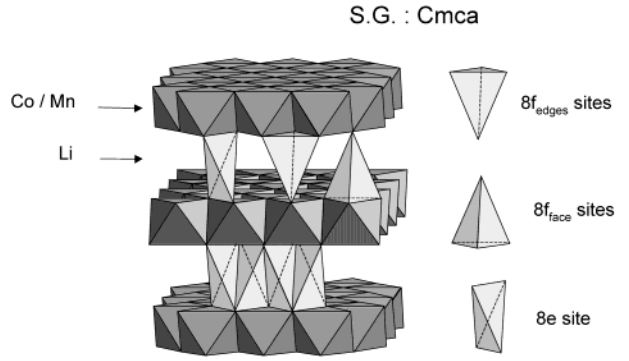

Figure 1. The $T^{\#}2$ stacking. The distorted sites available in the interslab space for the lithium ions are displayed.

$\leq x < 1$ lithium composition range.[3,4] Moreover, the Li// $T^{\#}2$-$Li_{2/3}Ni_{1/3}Mn_{2/3}O_2$ cells exhibit a $V = f(x)$ curve characterized by two potential domains and a useful $1/3 \leq x < 2/3$ cycling domain.

Recently, Shaju et al. studied chemical intercalation of lithium ions in $Li_{2/3}MO_2$ phases obtained by ion exchange in P2 sodium-containing phases. The addition of LiI after ion exchange in the molten salt mixture leads to the synthesis of $Li_{2/3+x}MO_2$ phases. These authors investigated especially the $Li_{2/3+x}Ni_{1/3}Mn_{2/3}O_2$[11] and $Li_{2/3+x}Co_{0.15}Mn_{0.85}O_2$[12] phases. The interest of this chemical lithiation resides in the formation of new materials that exhibit, for instance, for $Li_{2/3+x}Ni_{1/3}Mn_{2/3}O_2$, an electrochemical behavior characterized by a continuous variation of the potential within the [3.6−4.6 V] range. Indeed, the plateau normally observed for Li// $Li_{2/3}Ni_{1/3}Mn_{2/3}O_2$ at low voltage (2.8 V) has disappeared for Li//$Li_{2/3+x}Ni_{1/3}Mn_{2/3}O_2$. The useful reversible capacity is thus highly increased in the same potential domain, from 120 mA·h·g^{-1} for Li//$Li_{2/3}Ni_{1/3}Mn_{2/3}O_2$ to 170 mA·h.g^{-1} for Li//$Li_{2/3+x}Ni_{1/3}Mn_{2/3}O_2$.

Figure 1 represents a perspective view of the $T^{\#}2$-type structure, with two (Co, Mn)O_2 slabs per unit cell and in between, in the interslab space, the different tetrahedral sites (8e, $8f_{edges}$, and $8f_{face}$) that are available for the lithium ions. In our companion paper (part 1), by using neutron and electron diffraction, we have shown that, for $T^{\#}2$-$Li_{2/3}Co_{2/3}Mn_{1/3}O_2$ obtained by ion exchange of Na^+ by Li^+ in P2 sodium-containing phase, only the 8e and $8f_{edges}$ sites are occupied.[13] Furthermore, no ordering was evidenced between cobalt and manganese ions in the MO_2 slabs or between lithium ions and vacancies in the interslab space: a statistic distribution of the lithium ions was observed among the 8e and $8f_{edges}$ sites in the interslab space with the average ratio $8e/8f_{edges} \approx 2/3$. In this paper (part 2), we present the study of $T^{\#}2$-$Li_{2/3}Co_{2/3}Mn_{1/3}O_2$ as positive electrode material in lithium cells. Its electrochemical behavior is reported in detail, with also the characterization of the structural modifications that occur upon cycling.

Experimental Section

Electrochemistry. Electrochemical measurements were carried out at room temperature (25 °C) for the Li//$Li_x[Co_{2/3}Mn_{1/3}]O_2$ cells. The electrolyte used for the lithium batteries was 1 M $LiPF_6$ dissolved in a mixture of propylene carbonate (PC), ethylene carbonate (EC), and dimethyl carbonate (DMC) (1:1:3 by volume). The positive electrodes consisted of a mixture of 88 wt % of active material, 2% of PTFE (polytetrafluorethylene), and 10% of a mixture (1:1) of graphite and carbon black. The cells, assembled in an argon-filled drybox, were cycled at 400 μA·cm^{-2} (active mass = 15 mg, C/20 rate). The OCV measurements were carried out with a C/100 current density applied during 36 min steps and with an end relaxation criterion of $\Delta V/\Delta t = 1$ mV/h.

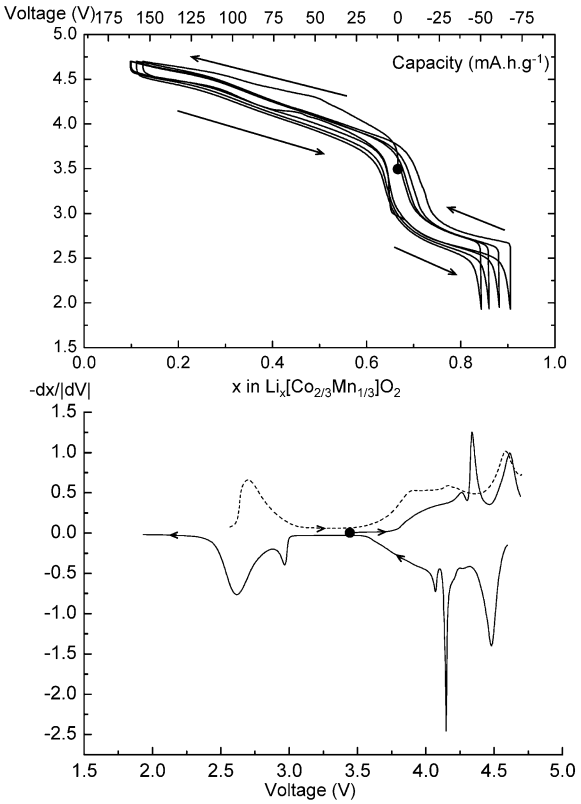

Figure 2. Cycling curve of an Li // $Li_{2/3}[Co_{2/3}Mn_{1/3}]O_2$ cell, measured during 4 cycles between 4.7 and 2.0 V. Differential $-dx/|dV| = f(V)$ curve of the first galvanostatic cycle (continuous line) and of the next charge (dashed line).

To synthesize a large amount of deintercalated $Li_xCo_{2/3}Mn_{1/3}O_2$ phases for structural characterization by using ex situ X-ray diffraction, cells were used with most of the positive electrodes consisting of pellets (ϕ = 8 mm, 600 MPa) of pure active material (~200 mg, no additive and no binder). Other positive electrodes that consisted of 90 wt % of active material and 10% of a mixture (1:1) of graphite and carbon black were used to synthesize the $Li_xCo_{2/3}Mn_{1/3}O_2$ with $x > 2/3$. All these cells were charged at low current density (C/200).

X-ray Diffraction. To identify the structural modifications that occur for $Li_xCo_{2/3}Mn_{1/3}O_2$ upon cycling, an in situ X-ray diffraction study was performed. A Swagelok specially designed cell was assembled with $T^{\#}2$-$Li_{2/3}Co_{2/3}Mn_{1/3}O_2$ as the positive electrode and Li metal as the negative electrode.[14] The cell was mounted on a SCINTAG diffractometer operating in Bragg−Brentano geometry, with Cu Kα radiation, and connected to a Mac-Pile system that supplied a galvanostatic mode (0.029 mA for 20.4 mg of active material) with 1-h relaxation periods every $\Delta x = 0.05$, during which XRD patterns were recorded.

The ex situ X-ray diffraction (XRD) patterns, recorded for structural characterization of the $Li_xCo_{2/3}Mn_{1/3}O_2$ phases by

(11) Shaju, K. M.; Rao, G. V. S.; Chowdari, B. V. R. *Electrochem. Commun.* **2002**, *4*, 633−638.
(12) Shaju, K. M.; Subba Rao, G. V.; Chowdari, B. V. R. *Solid State Ionics* **2002**, *152−153*, 69−81.
(13) Tournadre, F.; Croguennec, L.; Saadoune, I.; Weill, F.; Shao-Horn, Y.; Willmann, P.; Delmas, C. *Chem. Mater.* **2004**, *16*, 1411−1417.
(14) Morcrette, M.; Chabre, Y.; Vaughan, G.; Amatucci, G.; Leriche, J. B.; Patoux, S.; Masquelier, C.; Tarascon, J. M. *Electrochim. Acta* **2002**, *47*, 3137−3149.

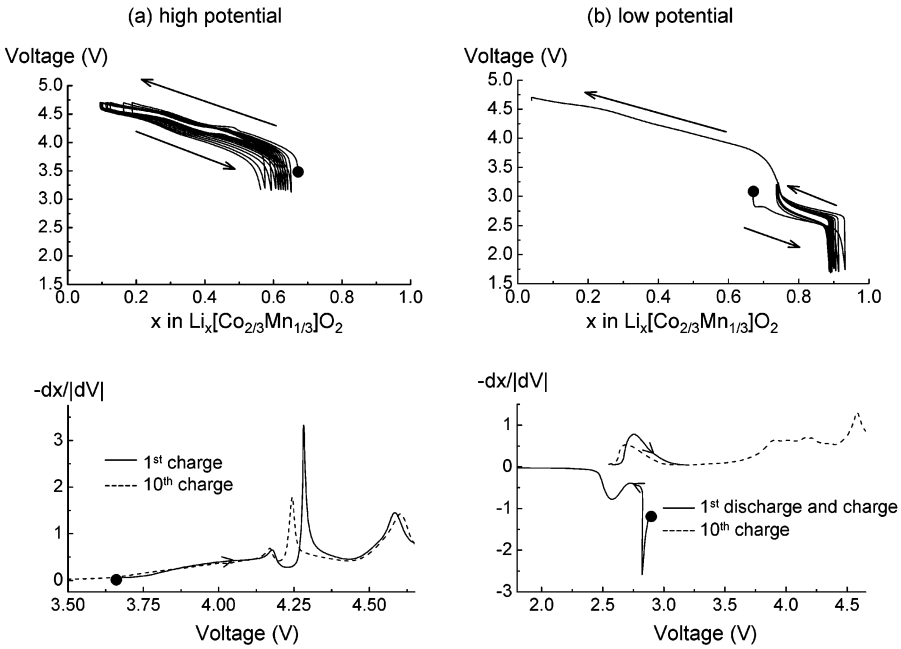

Figure 3. (a) Cycling curve of an Li // $Li_{2/3}[Co_{2/3}Mn_{1/3}]O_2$ cell measured during 10 cycles between 3.2 and 4.7 V. (b) Cycling curve of an Li // $Li_{2/3}[Co_{2/3}Mn_{1/3}]O_2$ cell measured during 10 cycles between 2.0 V and 3.0 V and a final charge from 2.0 V to 4.7 V. The derivative $-dx/|dV| = f(V)$ of the first cycle and of the 10th galvanostatic charge are also given.

the Rietveld method, were collected at room temperature from 5° to 120° (2θ) with a 0.02° step and a 40-s counting time by step, using a Siemens D5000 powder diffractometer with Cu Kα radiation and a graphite diffracted beam monochromator. The other ones were collected from 5° to 120° (2θ) with a 0.02° step and a 10-s counting time by step.

Results and Discussion

Electrochemical Properties. The electrochemical curve of Li//T#2-$Li_{2/3}Co_{2/3}Mn_{1/3}O_2$ and its derivative curve are given in Figure 2. Two potential ranges appear clearly on the electrochemical curve: the first one around 4.3 V corresponds to the Co^{4+}/Co^{3+} redox couple as observed in O2-$LiCoO_2$[7,8] and the second one around 2.8 V to the Mn^{4+}/Mn^{3+} couple as in O3-$LiMnO_2$.[15,16] 0.55 lithium ion is exchanged at high potential, with thus a 155 mA·h·g^{-1} reversible capacity at a C/20 rate. The second plateau in the 2.8-V region corresponds to a 65 mA·h·g^{-1} capacity with 0.23 lithium ion exchanged. As for the Li//O2-$LiCoO_2$ cells, the $V = f(x)$ curve profile is associated with the occurrence of several phase transitions upon cycling. These transformations can result from reversible $(Co_{2/3}Mn_{1/3})O_2$ sheet gliding, from lithium vacancies ordering, or from nonmetal to metal transition. As shown in Figure 2 by the peaks localized around 4.25, 4.35, and 4.65 V in the derivative curve, several phase transitions occur during the first charge (continuous line). The first two peaks are narrow and should correspond to first-order phase transition (i.e., to biphased domain), contrary to the third one which is broader. Because these peaks are also observed during the next discharge (continuous line), these transitions are reversible. Then, two other peaks appear around 2.95 and 2.6 V upon further lithium deintercalation. On the second charge (dashed line), the three peaks associated with the 2.95, 4.08, and 4.16 V discharge ones have disappeared. It appears thus that the phase transition that occurs during the first discharge at 2.9 V is irreversible and leads to an irreversible structural modification of the $Li_{2/3}Co_{2/3}Mn_{1/3}O_2$ system.

To better understand what is happening, other cycling conditions were used, with different potential limits. The corresponding galvanostatic curves and derivative curves ($-dx/|dV| = f(V)$) are given in Figure 3. Figure 3a shows the results obtained from a cell which was cycled 10 times, only in the high potential domain, between 3.2 and 4.7 V. The cell presented in Figure 3b was cycled 10 times only in the low potential domain, between 2.0 and 3 V, and then charged at high potential up to 4.7 V. When cycled into the high potential range almost no difference is observed between the first and the tenth cycles: only a fading of the intensity of the peaks observed at 4.20 and 4.30 V occurs. Upon cycling in the low potential range, an irreversible phase transition occurs around 2.8 V during the first discharge, leading to a different behavior afterward: indeed, contrary to what is observed in Figure 2, it seems that no first-order phase transition occurs anymore. However, with or without this irreversible phase transition, $Li_xCo_{2/3}Mn_{1/3}O_2$ exhibits a good cyclability with a useful capacity of 155 mA·h·g^{-1} in the $2.0 \leq V < 4.7$ V domain.

The open circuit voltage curves of two different batteries are reported in Figure 4. The first one corresponds to the deintercalation of lithium from $Li_{2/3}Co_{2/3}Mn_{1/3}O_2$ and the second one to the intercalation of lithium. Recording of the open circuit voltage curve yields more precise values of the potential because the conditions are chosen in order that the positive electrode material is as close as possible to the equilibrium: a more accurate observation of the voltage plateaus associated with first-order transition is thus possible. Upon charge, a small plateau is observed around $x = 0.5$, whereas a longer one is observed in the [0.39−0.48]

(15) Lee, Y. S.; Yoshio, M. *Electrochem. Solid-State Lett.* **2001**, *4*, A166.
(16) Capitaine, F. Thesis, Bordeaux I, 1997.

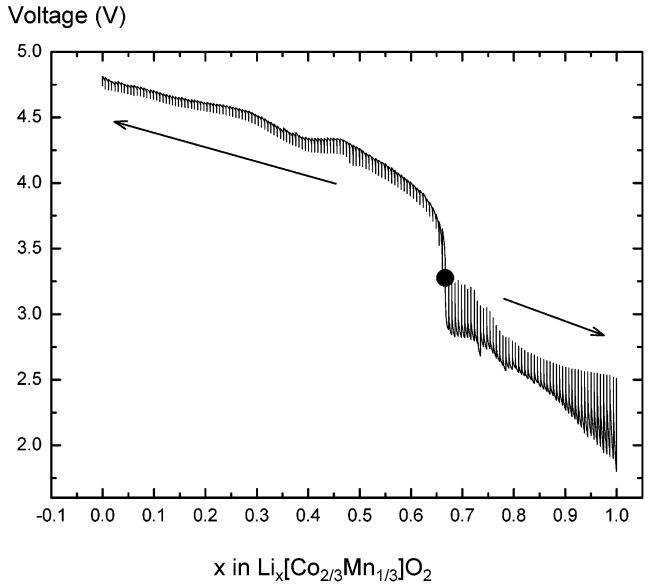

Figure 4. Open circuit voltage curve of two Li // $Li_{2/3}[Co_{2/3}Mn_{1/3}]O_2$ cells, one charged and one discharged, obtained with a C/100 current density applied for 36-min steps and an end relaxation criterion of $\Delta V/\Delta t = 1$ mV/h.

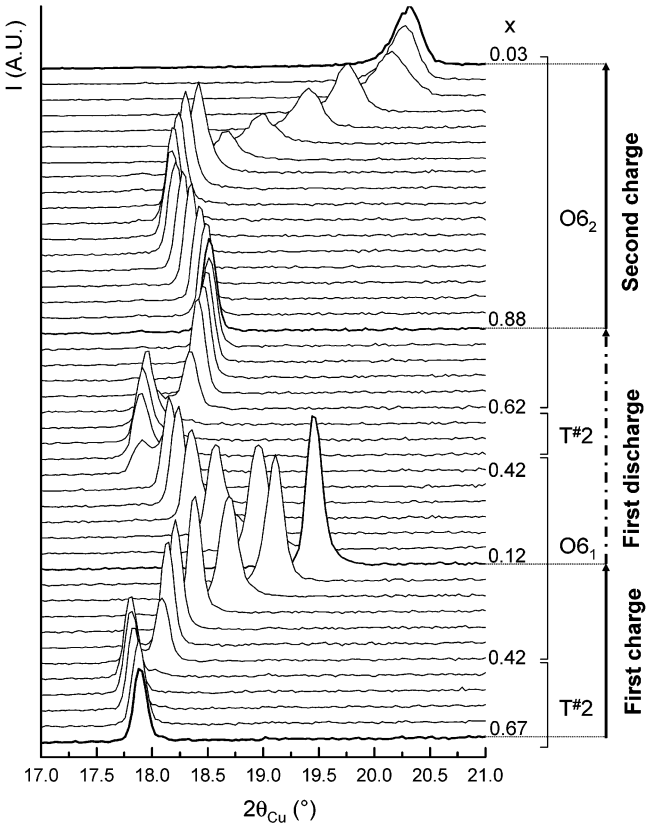

Figure 5. Evolution of the first X-ray diffraction peak versus lithium concentration in $Li_xCo_{2/3}Mn_{1/3}O_2$ obtained in situ by deintercalation of $T^{\#}2$-$Li_{2/3}Co_{2/3}Mn_{1/3}O_2$.

composition range. Upon discharge, a potential-like plateau is also observed in the $0.67 < x \leq 0.72$ composition range, but there is an "oscillation" of the potential at the end of the relaxation. This behavior suggests that the material equilibrium is difficult to reach or, in other words, that the cationic distribution is not well-defined. For x larger than 0.75, a more classical decrease of the potential, characteristic of a solid solution, is observed.

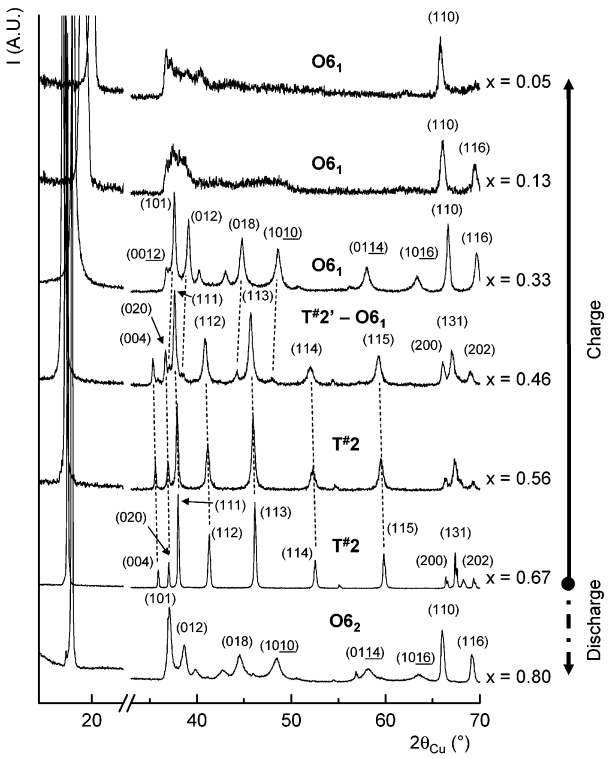

Figure 6. XRD patterns characteristic of each type of packing observed for the $Li_xCo_{2/3}Mn_{1/3}O_2$ system: the $T^{\#}2$-$Li_{2/3}Co_{2/3}Mn_{1/3}O_2$ starting phase, $T^{\#}2'$, $O6_1$, and $O6_2$ phases.

Note that a similar behavior was observed for O3-$LiMnO_2$ and was associated to manganese migration from the slab to the interslab space and thus to the spinel formation.[16] Indeed, during the migration, the material and, therefore, the potential are not at equilibrium. The open circuit voltage curve gives also information on the diffusion of the lithium in the structure, through the value of the polarization. A small polarization is observed upon charge, whereas a large one is observed upon discharge. At low potential, the amount of lithium in the host structure is already large ($x > 2/3$): further intercalation of lithium ions in the structure, and also their diffusion, become more and more difficult. Furthermore, if migration of cations occurs from the slab to the interslab space, the electrostatic repulsions in the interslab space increase, leading thus also to a strong decrease of the Li^+ diffusion.

XRD Study. *General Evolution.* To follow the structural modifications that occur upon cycling, in situ and ex situ XRD patterns of the $Li_xCo_{2/3}Mn_{1/3}O_2$ samples were recorded. Because all these phases exhibit XRD patterns characteristic of layered materials, the interslab distance (that is associated with the position of the first diffraction peak) is very sensitive to the amount of lithium in the structure and to the packing type. Therefore, in Figure 5, we have chosen to show for $Li_xCo_{2/3}Mn_{1/3}O_2$ the evolution recorded in situ of the first XRD peak versus lithium composition. During this experiment, the cell was first charged to 4.7 V, then discharged to 2.8 V, and finally charged again to 4.9 V. The lithium composition associated with these potentials are given on the right side of the figure. We can notice that this experiment shows the existence of one biphased domain (around $x = 0.42$) during the first charge and of two biphased domains (around $x = 0.42$

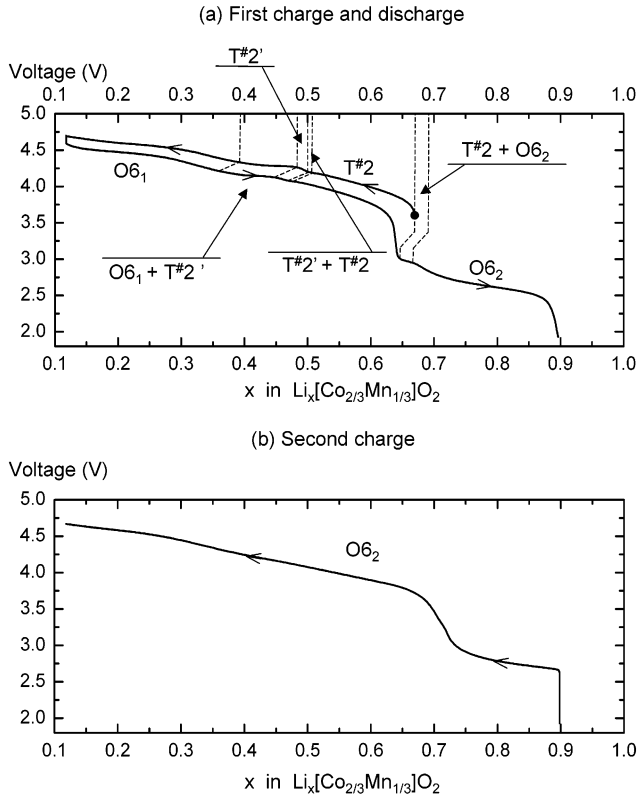

Figure 7. Phase diagram of the $Li_x[Co_{2/3}Mn_{1/3}]O_2$ system reported on the galvanostatic curve of an Li // T#2-$Li_{2/3}[Co_{2/3}Mn_{1/3}]O_2$ cell (a) before and (b) after the irreversible phase transition.

and $x = 0.62$) during the first discharge, one of those being associated with an irreversible transition. Only a large solid solution domain is observed afterward.

Ex situ XRD was also performed for materials selected as characteristic of each domain. Figure 6 shows the complete XRD patterns of these samples. Indeed, because of the difference in technology between positive electrodes, a film for in situ experiment and powder as pellet for ex situ XRD experiments, the XRD patterns are characterized by a strong preferential orientation for the former that prevents for instance any precise structural refinement by the Rietveld method. During the first charge, in a first step the T#2 structure is maintained, then an O6 structure, noted $O6_1$ in the next, is formed: this $O6_1$ structure is maintained for lithium amounts becoming negligible in the host structure, but with more and more stacking faults. During the first discharge, the T#2 structure disappears rapidly, leading to another O6 structure, noted $O6_2$ in the following. The main indexations of these XRD patterns are given in Figure 6, in *Cmca* and $R\bar{3}m$ space groups for the T#2 and O6 structures, respectively.

Figure 7a shows the first charge and discharge curves of an Li//$Li_{2/3}Co_{2/3}Mn_{1/3}O_2$ cell at C/20 rate, with an overview of the phase transitions. The different structures will be described in detail in the following. From $x = 2/3$ to $x = 0.12$, we observe several domains:

(a) $0.51 < x \leq 0.67$: T#2-$Li_xCo_{2/3}Mn_{1/3}O_2$ single-phase domain.

(b) $0.50 < x \leq 0.51$: two-phase domain, assigned to the T#2 → T#2′ transformation.

(c) $0.48 < x \leq 0.50$: T#2′-$Li_xCo_{2/3}Mn_{1/3}O_2$ single-phase domain.

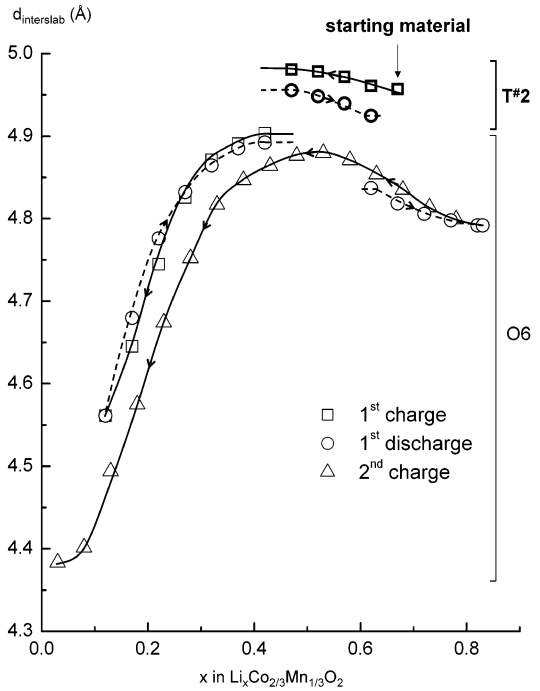

Figure 8. Evolution of the interslab distance (*c* parameter/number of sheets required to describe the cell) versus lithium concentration in $Li_xCo_{2/3}Mn_{1/3}O_2$.

(d) $0.39 < x \leq 0.48$: two-phase domain, assigned to the T#2′ → $O6_1$ transformation.

(e) $0.12 < x < 0.39$: $O6_1$-$Li_xCo_{2/3}Mn_{1/3}O_2$ single-phase domain.

In the first part of the discharge (i.e., for $0.12 < x \leq 0.67$), the same domains are observed whereas at lower potential, two other domains are observed:

(f) $0.67 < x \leq 0.69$: two-phase domain, assigned to the T#2′ → $O6_2$ transformation.

(g) $0.69 < x \leq 0.9$: $O6_2$-$Li_xCo_{2/3}Mn_{1/3}O_2$ single-phase domain.

After the formation of the $O6_2$ phase, the Li//$Li_xCo_{2/3}Mn_{1/3}O_2$ system behavior changes; indeed, the $O6_2$ structure is maintained in the whole [0.1−0.9] lithium composition range, as shown in Figure 7b.

Figure 8 presents for $Li_xCo_{2/3}Mn_{1/3}O_2$ the evolution of the interslab distance ($d_{interslab}$) upon cycling. The T#2-type structure exhibits the higher $d_{interslab}$ values (as shown with lines and symbols in bold on the figure). At the beginning of the first charge, in the T#2 single-phase domain, a small increase of $d_{interslab}$ is observed. Indeed, the removal of the lithium ions from the structure leads to an increase of the electrostatic repulsions between the oxygen layers: the lithium ions do not play their role of screening ions anymore. Upon further lithium deintercalation, with the formation of the $O6_1$ phase, a sudden decrease of $d_{interslab}$ occurs. It results from the difference in environment for lithium ions: octahedral environment in the $O6_1$ structure and very distorted tetrahedral one in the T#2 structure. A very similar difference in the interslab distances was observed between T#2- and O6-type phases for the O2-$LiCoO_2$ system.[8] Then, when lithium is deintercalated from the $O6_1$ phase, the structure becomes covalent enough, leading thus to a decrease of the electrostatic repulsions between the oxygen layers. Such a contraction of $d_{interslab}$ was already observed for other lamellar oxides at high

potential, for instance, for $Li_x(Ni, M)O_2$[17−19] and $Li_x(Co, M)O_2$.[20] During the next cell discharge, reintercalation of lithium ions in the structure leads to an evolution of $d_{interslab}$ as a function of the lithium composition similar to that observed upon charge, except in the $T^{\#}2$ single-phase domain where $d_{interslab}$ is surprisingly significantly smaller than for the starting $T^{\#}2$ phase. For further reintercalation of lithium in the structure, for $x > 0.67$, the formation of the $O6_2$ phase from the $T^{\#}2$ one leads to a decrease of $d_{interslab}$ due to the occupation of octahedral sites by lithium as it was previously discussed. For further lithium intercalation, the Li^+ ions play again their role of screening ions and allow a minimization of the electrostatic repulsions between the oxygen layers. During the second charge, the $O6_2$-type phase is maintained in the whole lithium composition range; the changes in interslab distance exhibit the classical evolution: increase due to the $O^{2-}-O^{2-}$ electrostatic repulsions in a first step and then strong decrease when the increase of the M−O bond covalency plays the predominant role.

Structural Characterization of $T^{\#}2$-$Li_xCo_{2/3}Mn_{1/3}O_2$ ($0.51 < x \leq 0.67$) and $T^{\#}2'$-$Li_xCo_{2/3}Mn_{1/3}O_2$ ($0.48 < x \leq 0.50$). At the beginning of the electrochemical deintercalation, the $T^{\#}2$-type packing is maintained up to $x = 0.48$. No significant difference was observed by XRD between the $T^{\#}2$ and the $T^{\#}2'$ structures; indeed, the variation of the interslab space distance is continuous in the [0.48−0.67] lithium composition range, showing no brutal variation of the $c_{orth.}$ cell parameter. This feature is totally similar to that observed for the same x value for the O2-Li_xCoO_2 system[8] and quite similar to that observed for the O3-Li_xCoO_2 system.[21] In this latter system, some of us have recently shown by using transmission electron microscopy that the monoclinic distortion observed in $Li_{0.5}CoO_2$ is due to a lithium/vacancy ordering in the interslab space.[22] Paulsen et al. have therefore suggested that one can also expect a lithium/vacancy ordering for $x = 0.50$ in the O2-Li_xCoO_2 system.[3]

A refinement by the Rietveld method of the XRD pattern of $T^{\#}2'$-$Li_{0.48}Co_{2/3}Mn_{1/3}O_2$ was thus done in the *Cmca* orthorhombic space group, where the cobalt and manganese ions occupy statistically the 4a (0, 0, 0) position and oxygen the 8f (0, y, z) position. As we cannot determine the lithium ion position by XRD, we fixed it in the 8e ($^1/_4$, y, $^1/_4$) site, the occupancy being 0.24 (i.e., 0.48/2). Note that for $T^{\#}2'$-$Li_{0.48}Co_{2/3}Mn_{1/3}O_2$ we chose to fix Li only in the 8e site by similarity to recent results obtained by some of us for $T^{\#}2$-$Li_{0.56}CoO_2$.[9] Furthermore, first-principle ab initio calculations have also shown that for $x = 0.50$ the Li^+ ions are stabilized in the 8e site only in those structures. The cell parameters, the profile parameters of the pseudo-Voigt function, the

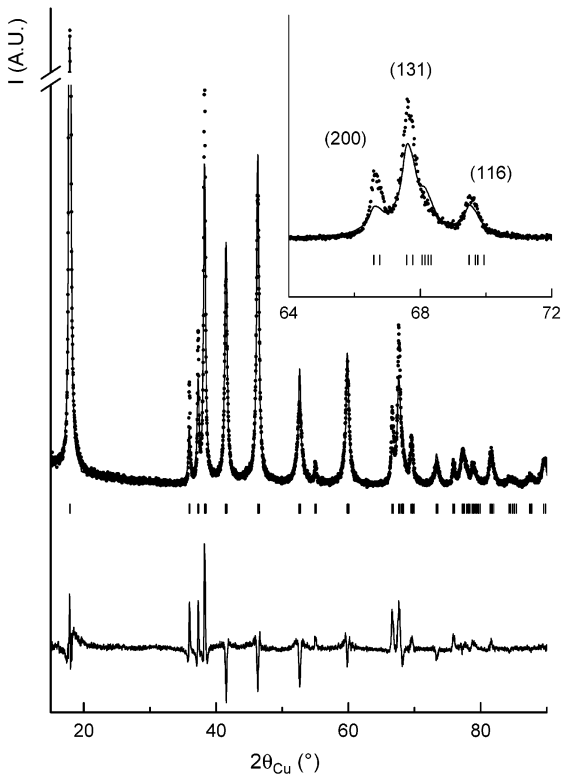

Figure 9. Observed and calculated X-ray diffraction profiles for a $T^{\#}2'$-$Li_{0.48}Co_{2/3}Mn_{1/3}O_2$ phase: (●) observed; (−) calculated; lower trace: difference plot; bars: reflections.

preferential orientation along the $c_{orth.}$-axis, the y and z atomic positions of oxygen, the y atomic position of lithium, and the atomic displacement parameters of cobalt, manganese, and oxygen were refined. The lithium atomic displacement parameter was fixed to a value usually observed in layered oxides (1.2 Å^2).[23] The experimental and calculated diffractograms are represented in Figure 9. The results of this refinement are given in Table 1. The reliability factors ($R_{wp} = 17.6\%$; $R_B = 5.0\%$) obtained for the Rietveld refinement are rather good. But the difference $|I_{obs.} - I_{calc.}|$ is not well-minimized because the peak profile is not fully satisfactorily simulated using a pseudo-Voigt function as the XRD pattern does not exhibit peak widths that strictly vary smoothly as a function of the scattering angles. The refinement shows also that the particles exhibit a weak tendency to be oriented perpendicularly to the c-axis (Table 1), in agreement with the platelike shape of the particles of the starting phase.[6,7]

In comparison to the starting material $T^{\#}2$-$Li_{2/3}Co_{2/3}Mn_{1/3}O_2$,[13] $T^{\#}2'$-$Li_{0.48}Co_{2/3}Mn_{1/3}O_2$ is characterized by longer M−M distances and shorter M−O distances as shown in Table 2. Note that, in the $T^{\#}2$ and $T^{\#}2'$ domains, the M−M distances are always shorter than the minimum R_c empirical critical value described by J. B. Goodenough[24] ($R_c = 2.853$ for $x = 2/3$ and $R_c = 2.848$ for $x = 0.48$). Since the bands are not full, an electronic delocalization is thus possible through the overlapping of the $t_{2g}-t_{2g}$ orbitals, this overlapping being possible in such a type of material where the octahedra share edges in the slabs. At the same time,

(17) Prado, G.; Rougier, A.; Fournès, L.; Delmas, C. *J. Electrochem. Soc.* **2000**, *147*, 2880.
(18) Pouillerie, C.; Croguennec, L.; Delmas, C. *Solid State Ionics* **2000**, *132*, 15−29.
(19) Croguennec, L.; Pouillerie, C.; Mansour, A. N.; Delmas, C. *J. Mater. Chem.* **2001**, *11*, 131−141.
(20) Van der Ven, A.; Aydinol, M. K.; Ceder, G.; Kresse, G.; Hafner, J. *Phys. Rev. B* **1998**, *58*, 2975−2987.
(21) Reimers, J. N.; Dahn, J. R. *J. Electrochem. Soc.* **1992**, *139*, 2091−2097.
(22) Shao-Horn, Y.; Weill, F.; Levasseur, S.; Delmas, C. *J. Electrochem. Soc.* **2003**, *150*, A366.
(23) Rougier, A.; Saadoune, I.; Gravereau, P.; Willmann, P.; Delmas, C. *Solid State Ionics* **1996**, *90*, 83.
(24) Goodenough, J. B. *Prog. Solid State Chem.* **1971**, *5*, 278−279.

Table 1. Structural Parameters Determined by the Rietveld Refinement of the X-ray Diffraction Data Recorded for T#2′-$Li_{0.48}Co_{2/3}Mn_{1/3}O_2$[a]

space group: *Cmca*
$a_{orth.}$ = 2.8171(1) Å
$b_{orth.}$ = 4.8559(2) Å
$c_{orth.}$ = 10.0624(4) Å

atom	site	Wyckoff positions			occupancy	B (Å^2)
Li (1)	8e	1/4	0.40(3)	1/4	0.24	1.2
Co	4a	0	0	0	2/3	0.9(6)
Mn	4a	0	0	0	1/3	0.9(6)
O	8f	0	0.842(3)	0.595(2)	1	1.5(4)

Distances (Å)

d_{M-M}	2.81(1) ×4 /2.82(1) ×2
d_{M-O}	1.92(1) ×4/1.87(2) ×2
d_{Li8e-O}	2.12(2) ×2/2.08(2) ×2

Conditions of the Run

temperature	300 K
angular range	5° ≤ 2θ ≤ 120°
step scan increment (2θ)	0.02°
sample displacement correction	0.280(1)°
number of fitted parameters	18

Profile Parameters

pseudo-Voigt function	η_0 = 0.14(5)
PV = ηL+(1 − η)G with $\eta = \eta_0 + X(2\theta)$	
half-width parameters	X = 0.008(3) U = −0.25(4) V = 0.48(8) W = −0.04(1)
preferential orientation of the particles perpendicular to the *c*-axis:	1.045(2)

Conventional Rietveld R-Factors for Points with Bragg Contribution
R_{wp} = 17.6%; R_B = 5.0%

[a] Note: Standard deviations have been multiplied by the Scor number (3.70) to correct from local correlations.

Table 2. Interatomic Distances Calculated for the T#2-$Li_{2/3}Co_{2/3}Mn_{1/3}O_2$ and the T#2′-$Li_{0.48}Co_{2/3}Mn_{1/3}O_2$ Phases

distances	T#2-$Li_{2/3}Co_{2/3}Mn_{1/3}O_2$	T#2′-$Li_{0.48}Co_{2/3}Mn_{1/3}O_2$
M−M (Å)	2.80(2) ×4; 2.81(2) ×2	2.81(1) ×4; 2.82(1) ×2
M−O (Å)	1.91(1) ×6	1.92(1) ×4; 1.87(1) ×2
Li−O (Å)	2.10(2) ×2; 2.00(2) ×2	2.12(2) ×4; 2.08(2) ×2

because of the increase of the electrostatic repulsions between the oxygen layers upon deintercalation, the Li−O distances increase (Table 2).

Structural Evolution of O6$_1$-$Li_xCo_{2/3}Mn_{1/3}O_2$ (0.12 < x ≤ 0.39). The XRD pattern of $Li_{0.33}Co_{2/3}Mn_{1/3}O_2$ is characteristic of the O6 stacking that is stabilized at high potential in the [0.12−0.39] lithium composition range. As shown by the perspective view given in Figure 10, the unusual O6 structure can be described by six MO_2 slabs packed along the *c*-axis. All the LiO_6 octahedra share on one side a face with MO_6 octahedra and three edges on the other side, like in the O2 structure.[7] However, the existence of two different types of MO_2 slabs differentiates the O6 structure. In the first type of MO_2 slabs, MO_6 octahedra share only faces with LiO_6 ones, while in the second one, the MO_6 octahedra share only edges with LiO_6 ones.

The O6 stacking is described using the $R\bar{3}m$ space group, where the lithium ions occupy octahedral sites (6c position) and where two different cobalt/manganese layers (Co(1)/Mn(1) in 3a and Co(2)/Mn(2) in 3b) exist. There are also two types of oxygen ions: O(1) and O(2), both in 6c positions. We refined the XRD pattern of one

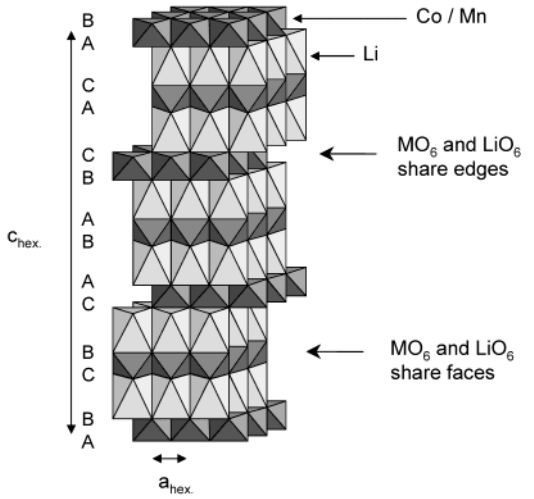

Figure 10. O6 stacking.

O6 phase, $Li_{0.33}Co_{2/3}Mn_{1/3}O_2$, by the Rietveld method. As the X-ray diffraction is a method that does not allow localization of lithium ions in a heavy host structure, their position was fixed in 6c (0, 0, 1/12), the site occupancy being 0.33 and the 1/12 value for *z* corresponding to the middle position of the interslab space. But as the LiO_6 octahedra are not symmetric, they share one face with a CoO_6 octahedron on a side and edges with CoO_6 octahedra on the other side, the normal lithium ions position is thus slightly different from z = 1/12. The atomic positions to be refined are the *z* coordinates of oxygens. We also refined the preferential orientation along the $c_{hex.}$ axis and the cobalt, manganese, and oxygen atomic displacement parameters. The lithium atomic displacement parameter was fixed to a value usually observed in such compounds (1.2 Å^2).[25] The experimental and calculated diffractograms are shown in Figure 11. The results are given in Table 3. The refinement shows that the particles exhibit a preferential orientation along the $c_{hex.}$ axis, in good agreement with their platelike shape (Table 3). In this structure, with cobalt and manganese in the two 3a and 3b crystallographic sites, each independent oxygen position gives rise to two oxygen layers belonging to the same $(Co_{2/3}Mn_{1/3})O_2$ sheet so that the space group chosen allows differentiation of the $(Co_{2/3}Mn_{1/3})O_2$ layers. The octahedra-sharing faces with LiO_6 exhibit a 1.873(3) Å M−O distance, whereas the octahedra-sharing edges with LiO_6 exhibit a 1.867(3) Å M−O distance. Mendiboure et al. previously suggested that, for O6-Li_xCoO_2, the existence of these two different MO_2 slabs could be due to a charge ordering of the Co^{4+} and Co^{3+} ions between these two different slabs. The trivalent cobalt ions could be mainly segregate in the sheets in which CoO_6 octahedra share faces with LiO_6 ones, while the tetravalent cobalt would be in the sheets in which CoO_6 octahedra share edges with LiO_6 ones. Carlier et al. have investigated the $Li_{0.5}CoO_2$ and $Li_{0.33}CoO_2$ compositions by spin-polarized calculations but no such ordering was predicted.[10] Moreover, in the mixed cobalt/manganese lithium oxide, a charge ordering of the Co^{3+}, Co^{4+}, and Mn^{4+} is not possible as the Co^{3+} and Mn^{4+} were not ordered in the starting T#2-$Li_xCo_{2/3}Mn_{1/3}O_2$ material.

(25) Rougier, A.; Gravereau, P.; Delmas, C. *J. Electrochem. Soc.* **1996**, *143*, 1168−1174.

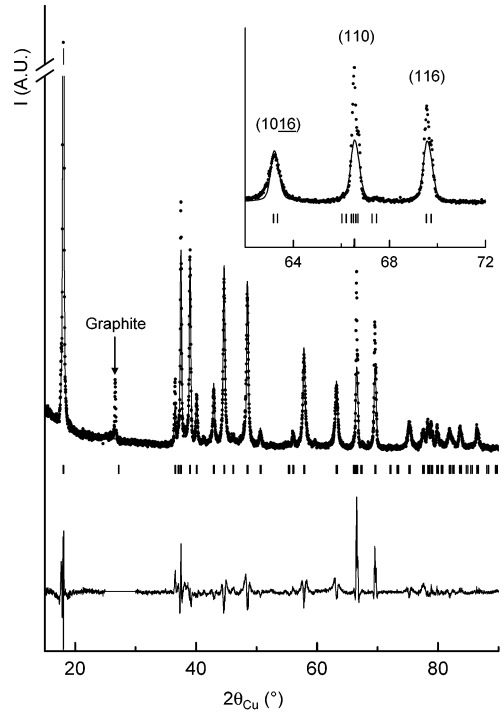

Figure 11. Observed and calculated X-ray diffraction profiles for an $O6_1$-$Li_{0.33}Co_{2/3}Mn_{1/3}O_2$ phase: (●) observed; (−) calculated; lower trace: difference plot; bars: reflections.

The segregation of the trivalent and tetravalent metal ions cannot explain the formation of the O6 structure.

Structural Evolution of $O6_2$-$Li_xCo_{2/3}Mn_{1/3}O_2$ ($0.69 < x \leq 0.90$). The $O6_2$-$Li_xCo_{2/3}Mn_{1/3}O_2$ structure is formed at low potential (~2.8 V) on the first discharge of the Li//$Li_{2/3}Co_{2/3}Mn_{1/3}O_2$ cell and is then maintained in the whole cycling range (Figures 5 and 6). Figure 12 shows the comparison of the XRD patterns of the $O6_1$ and $O6_2$ phases for $x = 0.33$ and $x = 0.80$, respectively. The XRD pattern of the $O6_2$-$Li_{0.80}Co_{2/3}Mn_{1/3}O_2$ can be totally indexed in the $R\bar{3}m$ space group with $a = 2.812(5)$ Å and $c = 29.0387(4)$ Å, but the peak width does not vary smoothly as a function of the scattering angle: while the (00*l*) and (11*l*) diffraction lines are narrow, the (10*l*) and (01*l*) ones are broadened. Therefore, only a refinement of the cell parameters using the full pattern matching method has been achieved. The comparison of the experimental and calculated XRD patterns is shown in Figure 13.

To our knowledge, it is the first time that an "O6" structure is observed in the $0.67 < x \leq 1$ lithium composition range. Moreover, as the formation of $O6_2$ is irreversible contrary to that of $O6_1$, there must exist a structural difference between these two phases. Unfortunately, as $O6_2$ exhibits a faulted structure, neutron and X-ray diffraction were not sufficient to fully solve its structure.

The intercalation of lithium ions in $T^{\#}2$-$Li_{2/3}Co_{2/3}$-$Mn_{1/3}O_2$ induces the reduction of Mn^{4+} in Mn^{3+}: because of the Jahn−Teller effect (Mn^{3+} d^4: t_{2g}^3 e_g^1), the $Mn^{3+}O_6$ octahedra are distorted with four short and two long Mn^{3+}−O distances. The Mn^{3+} ions are thus highly unstable in the highly symmetrical surrounding of the $(Co^{3+}_{2/3}Mn^{4+}_{1/3})O_2$ slabs. There is therefore at the beginning of the reduction a strong driving force for Mn^{3+} dismutation ($2Mn^{3+} \rightarrow Mn^{4+} + Mn^{2+}$) that allows the migration of the formed Mn^{2+} slabs ions from the slab to the interslab space and the stabilization of the formed Mn^{4+} ions in the MO_2 slabs. As shown by the OCV electrochemical curve in Figure 4, this migration is supported by the "oscillation" of the relaxation potential in the [0.67−0.69] lithium composition range,[16] which shows that the cationic distribution is not well-defined as the energy of this material does not vary linearly with the composition. The "oscillation" of the potential corresponds to the intercalation of 0.02 lithium ions and to the reduction of 0.02 Mn^{4+} in Mn^{3+} ions, and thus to the possible migration of 0.01 Mn^{2+} ions from the slab to the interslab space. Note that 0.01 corresponds to 3%

Table 3. Structural Parameters Determined by the Rietveld Refinement of the X-ray Diffraction Data Recorded for $O6_1$-$Li_{0.33}Co_{2/3}Mn_{1/3}O_2$[a]

space group: $R\bar{3}m$
$a_{hex.} = 2.811(3)$ Å
$c_{hex.} = 29.556(3)$ Å

atom	site	Wyckoff positions			occupancy	B (Å^2)
Li	6c	0	0	$^1/_{12}$	0.33	1.2
Co(1)	3a	0	0	0	$^2/_3$	0.5(2)
Mn(1)	3a	0	0	0	$^1/_3$	0.5(2)
Co(2)	3b	0	0	$^1/_2$	$^2/_3$	0.5(2)
Mn(2)	3b	0	0	$^1/_2$	$^1/_3$	0.5(2)
O(1)	6c	0	0	0.198(6)	1	1.9(3)
O(2)	6c	0	0	0.365(6)	1	1.9(3)

Distances (Å)

d_{M-M}	2.81(1) ×6
d_{M3a-O}	1.873(6) ×6
d_{M3b-O}	1.867(6) ×6
d_{Li-O}	2.37(3) ×3/2.10(4) ×3

Conditions of the Run

temperature	300 K
angular range	$5° \leq 2\theta \leq 120°$
step scan increment (2θ)	0.02°
sample displacement correction	0.058(2)°
number of fitted parameters	16

Profile Parameters

pseudo-Voigt function	$\eta_0 = 0.58(8)$
PV = $\eta L + (1-\eta)G$ with $\eta = \eta_0 + X(2\theta)$	$X = 0.0007(1)$
	$U = -0.11(2)$
half-width parameters	$V = 0.27(3)$
	$W = -0.018(5)$
preferential orientation of the particles perpendicular to the *c*-axis:	1.027(9)

Conventional Rietveld *R*-Factors for Points with Bragg Contribution
$R_{wp} = 25.2\%$; $R_B = 8.67\%$

[a] Note: Standard deviations have been multiplied by the Scor number (3.14) to correct from local correlations.

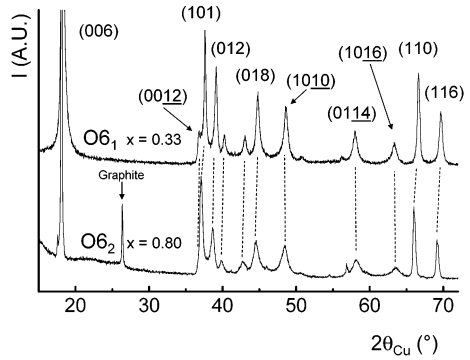

Figure 12. Comparison of the X-ray diffraction patterns for an $O6_1$-$Li_{0.33}Co_{2/3}Mn_{1/3}O_2$ and an $O6_2$-$Li_{0.80}Co_{2/3}Mn_{1/3}O_2$ phase.

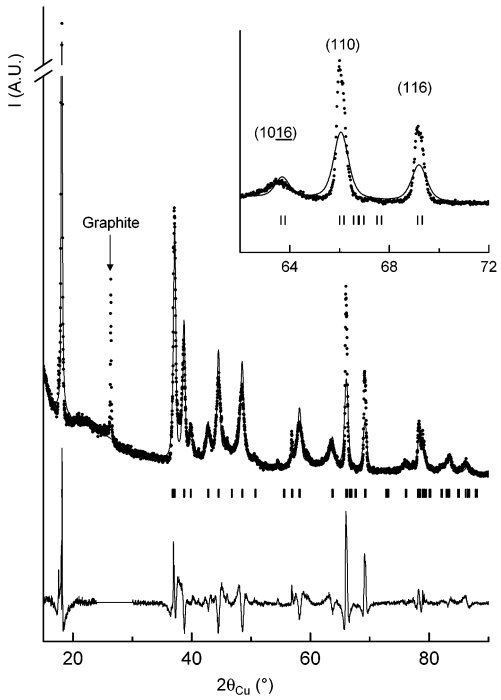

Figure 13. Observed and calculated X-ray diffraction profiles for an $O6_2$ phase: (●) observed; (−) calculated; lower trace: difference plot; bars: reflections.

of the total manganese amount in the material. It appears that only a small amount of manganese ions would have moved from the slab to the interslab space: after the formation of $O6_2$, the migration is rapidly stopped. It is in good agreement with the following two points:

(a) With further reduction of the material, the proportion of Mn^{3+} ions versus Co^{3+} and Mn^{4+} ions increases in the slab, leading to a higher stabilization of these ions without any need for dismutation and migration.

(b) Because further reduction of the material goes with an increasing amount of lithium ions in the interslab space, very rapid stabilization of manganese ions in the interslab space sites becomes no more possible because of strong electrostatic repulsion between the manganese and the lithium ions.

The formation of $O6_2$ with the possible presence of manganese ions in the interslab space that would link the slabs all together prevents the formation of the $T^{\#}2$-stacking in the following charge.

Conclusion

The $T^{\#}2$-$Li_{2/3}Co_{2/3}Mn_{1/3}O_2$ phase exhibits good electrochemical performances with a capacity of 220 $mA{\cdot}h{\cdot}g^{-1}$ divided into two voltage domains. As the potential in the $0.67 < x \leq 1$ lithium composition range (about 2.8 V) is too low for Li-ion batteries applications, the efficient capacity is 155 $mA{\cdot}h{\cdot}g^{-1}$ with an average potential of 4.3 V. Several transitions occur upon cycling and one of them, corresponding to the formation of $O6_2$-$Li_xCo_{2/3}Mn_{1/3}O_2$, is irreversible. The electrochemical behavior (capacity and cyclability) is not altered by this phase transition. This irreversible transition could be due to cationic migrations from the slab to the interslab space; divalent manganese ions could migrate after dismutation.

Acknowledgment. The authors wish to thank Cathy Denage for technical assistance and CNES and Région Aquitaine for financial support.

CM035177H